The Effect of Compressibility on Barotropic and Baroclinic Instability

BRIAN D. GROSS

Geophysical Fluid Dynamics Laboratory/NOAA, Princeton University, Princeton, New Jersey

(Manuscript received 16 October 1995, in final form 20 May 1996)

ABSTRACT

The effect of compressibility on two-dimensional barotropic and baroclinic growth rates is examined by means of a linearized nonhydrostatic compressible model. It is shown that the growth rates are diminished when compressibility is included because perturbation internal energy resents a sink of basic-state kinetic energy when work is done to compress the medium. Nonlinear simulations provided by compressible and incompressible versions of the ZETA model show that the solutions are nearly identical, but the compressible solution develops more slowly than the incompressible one, consistent with the linear analysis.

1. Introduction

Numerical models of geophysical flows characterized by large horizontal scales traditionally employ the hydrostatic approximation. This approximation removes vertically propagating acoustic waves, although care must be taken to properly account for Lamb waves. For flows of small horizontal scale such as convection, compressible nonhydrostatic models are becoming more popular (e.g., Chen 1991; Held et al. 1993) because they can be integrated nearly as efficiently as filtered models (e.g., using the anelastic system) without any of the physical assumptions or computational complexity often associated with them. Further efficiency can be achieved in these compressible models by explicitly decreasing the phase speed of the acoustic wave, thereby allowing a larger time step. This assumes that the acoustic modes are unimportant in determining the principal flow characteristics.

The purpose of this paper is to examine the effects of compressibility on flows of intermediate horizontal scale or flows that possess multiple scales, such as a developing baroclinic wave with an imbedded front. In these types of flows it is often desirable to capture nonhydrostatic effects while retaining the efficiency and accuracy of a fully compressible model. Here, barotropic and baroclinic instability in a fully compressible atmosphere will be examined. It will be shown that the growth rates can be quite sensitive to the degree of compressibility, as measured by the ratio of the length scale to a deformation radius based on the acoustic phase speed. One consequence of this sensitivity is that the full value of the sound speed must be used to accurately simulate these flows.

The nonhydrostatic compressible linear system is developed and nondimensionalized in section 2. Barotropic and baroclinic linear growth rates are derived in sections 3 and 4, respectively, and fully nonlinear simulations of these instabilities with a new nonhydrostatic compressible version of the ZETA model (Orlanski and Gross 1994) are presented in section 5. A summary and conclusions are provided in section 6.

2. Linear growth rates

The compressible nonhydrostatic equations for adiabatic inviscid motion on a β plane are

$$\frac{d\mathbf{v}_H}{dt} = -\theta\nabla P - f\,\mathbf{k}\times\mathbf{v}_H \tag{2.1}$$

$$\frac{dw}{dt} = -\theta\frac{\partial P}{\partial z} - g \tag{2.2}$$

$$\frac{dP}{dt} = -\frac{c_s^2}{\theta}\nabla\cdot\mathbf{v} \tag{2.3}$$

$$\frac{d\theta}{dt} = 0, \tag{2.4}$$

where $\mathbf{v}_H$ and w are the horizontal and vertical velocities respectively, θ is the potential temperature, the pressure variable is $P \equiv c_p(p/p_0)^{R/c_p}$, the Coriolis parameter is $f = f_0 + \beta_0 y$, and $c_s^2 = (c_p/c_v)RT = (R/c_v)\theta P$ is the sound speed squared at temperature T. Gravitational acceleration, the gas constant, and the specific heats are denoted

Corresponding author address: Dr. Brian D. Gross, NOAA/GFDL, Princeton University, P.O. Box 308, Forrestal Campus, U.S. Route 1, Princeton, NJ 08542.
E-mail: bdg@gfdl.gov

by their usual symbols. Linearizing about a zonal flow $\bar{u}(y, z)$ in geostrophic balance, given by

$$f\bar{u} = -\bar{\theta}\frac{\partial}{\partial y}\bar{P}, \tag{2.5}$$

and hydrostatic balance, given by

$$\frac{\partial}{\partial z}\bar{P} = -\frac{g}{\bar{\theta}}, \tag{2.6}$$

results in

$$Du' = -\bar{\theta}\frac{\partial}{\partial x}P' + fv' - \mathbf{v}\cdot\nabla\bar{u} \tag{2.7}$$

$$Dv' = -\bar{\theta}\frac{\partial}{\partial y}P' - fu' + \frac{f\bar{u}}{g}b' \tag{2.8}$$

$$Dw' = -\bar{\theta}\frac{\partial}{\partial z}P' + b' \tag{2.9}$$

$$DP' = -\frac{\bar{c}_s^2}{\bar{\theta}}\left[\nabla\cdot\mathbf{v}' + \frac{c_v}{R}\mathbf{v}\cdot\nabla \ln \bar{P}\right] \tag{2.10}$$

$$Db' = -N^2w' + \left(\bar{u}_z - \frac{N^2}{g}\bar{u}\right)fv', \tag{2.11}$$

where $b' = g\theta'/\bar{\theta}$ is the bouyancy and

$$D(\ ) = \frac{\partial}{\partial t}(\ ) + \bar{u}\frac{\partial}{\partial x}(\ ). \tag{2.12}$$

Overbars denote the basic-state and primes denote deviations from this state. Thermal wind balance has been used in (2.11) to express the basic-state potential temperature gradient in terms of $\bar{u}(y, z)$.

Introducing the scales L and H for the horizontal and vertical independent variables and $(\bar{u}, \bar{\theta}, \mathbf{v}_H', w', P', b') \sim O(U, \Theta, V, VH/L, f_0VL/\Theta, f_0VL/H)$ for the dependent variables allows the nondimensional equations to be written as

$$\mathrm{Ro}Du' = -\bar{\theta}\frac{\partial}{\partial x}P' + fv' - \mathrm{Ro}\mathbf{v}'\cdot\nabla\bar{u} \tag{2.13}$$

$$\mathrm{Ro}Dv' = -\bar{\theta}\frac{\partial}{\partial y}P' - fu' + F_E^2\mathrm{Ro}\,f\bar{u}b' \tag{2.14}$$

$$\left(\frac{H}{L}\right)^2\mathrm{Ro}Dw' = -\bar{\theta}\frac{\partial}{\partial z}P' + b' \tag{2.15}$$

$$F_c^2\mathrm{Ro}D(\bar{\theta}P') = -\frac{\bar{c}_s^2}{c_0^2}\nabla\cdot\mathbf{v}' - F_c^2\mathrm{Ro}\mathbf{v}'\cdot\,\bar{\theta}\nabla\bar{P} \tag{2.16}$$

$$F_I^2\mathrm{Ro}Db' = -\frac{N^2}{N_0^2}w' + \mathrm{Ro}(F_I^2\bar{u}_z - F_E^2\bar{u})fv', \tag{2.17}$$

where c_0 is a characteristic sound speed, $f = 1 + \mathrm{Ro}\beta y$, $\beta = \beta_0L^2/U$, the Rossby number is $\mathrm{Ro} = U/(f_0L)$, and

$$(F_c, F_I, F_E) = \left(\frac{f_0L}{c_0}, \frac{f_0L}{N_0H}, \frac{f_0L}{\sqrt{gH}}\right) \tag{2.18}$$

represent ratios of the length scale to different deformation radii. The first of these, $F_c = f_0L/c_0$, is zero in incompressible, Boussinesq, or anelastic flow. Although the ratios defined in (2.18) appear only in combination with Ro in (2.13)–(2.17), the discussion of the results presented in the following section is clearer when these ratios remain distinct.

The last terms on the right-hand sides of (2.14) and (2.17) represent buoyancy oscillations in the meridional direction due to sloping basic-state isentropes. The restoring force is associated with the meridional pressure gradient. These terms are neglected in the Boussinesq and anelastic approximations and can be neglected with the present scaling if $\mathrm{Ro}F_E^2 \ll 1$, which will be assumed here. With this assumption, the set of nondimensional equations to be considered is

$$\mathrm{Ro}Du' = -\bar{\theta}\frac{\partial}{\partial x}P' + fv' - \mathrm{Ro}\mathbf{v}\cdot\nabla\bar{u} \tag{2.19}$$

$$\mathrm{Ro}Dv' = -\bar{\theta}\frac{\partial}{\partial y}P' - fu' \tag{2.20}$$

$$\left(\frac{H}{L}\right)^2\mathrm{Ro}Dw' = -\bar{\theta}\frac{\partial}{\partial z}P' + b' \tag{2.21}$$

$$F_c^2\mathrm{Ro}D(\bar{\theta}P') = -\frac{\bar{c}_s^2}{c_0^2}\nabla\cdot\mathbf{v}' - F_c^2\mathrm{Ro}\mathbf{v}'\cdot\bar{\theta}\nabla\bar{P} \tag{2.22}$$

$$F_I^2\mathrm{Ro}Db' = -\frac{N^2}{N_0^2}w' + F_I^2\mathrm{Ro}\bar{u}_2fv'. \tag{2.23}$$

These equations will be used to examine the growth rates of barotropic and baroclinic instability, with a focus on how the growth rates depend on the parameter F_c.

3. Barotropic modes

Consider an isentropic barotropic current $\bar{u}(y)$ at potential temperature θ_0 bounded by rigid walls and a rigid lid. Adiabatic barotropic perturbations to this current are governed by

$$\mathrm{Ro}Du' = -\frac{\partial}{\partial x}\varphi' + (f - \mathrm{Ro}\bar{u}_y)v' \tag{3.1}$$

$$\mathrm{Ro}Dv' = -\frac{\partial}{\partial y}\varphi' - fu' \tag{3.2}$$

$$F_c^2\mathrm{Ro}D\varphi' = -\tilde{c}_s^2(y)\nabla_H\cdot\mathbf{v}' + F_c^2\mathrm{Ro}\,f\bar{u}v' \tag{3.3}$$

with w' and θ' identically zero. The vertically averaged nondimensional sound speed is $\tilde{c}_s$, and the pressure variable is $\varphi' = \theta_0P'$. The equation set (3.1)–(3.3) is isomorphic to the linearized shallow water equations in a rotating reference frame, with F_E replaced by F_c and the surface wave phase speed replaced by the speed of sound. Assuming solutions of the form

$$[u', v', \varphi'] = [U, V, \Phi](y)e^{i\alpha(x-ct)} \tag{3.4}$$

allows the derivation of a single equation for V:

$$\frac{d}{dy}\left[\frac{\tilde{c}_s^2\left\{(\bar{u}-c)\frac{dV}{dy}-\bar{u}_y V\right\}-\mathrm{Ro}F_c^2 f\bar{u}(\bar{u}-c)V}{\tilde{c}_s^2-[M(\bar{u}-c)]^2}\right]$$
$$+\left[\mathrm{Ro}F_c^2 f\frac{d}{dy}\left[\frac{\tilde{c}_s^2}{\tilde{c}_s^2-[M(\bar{u}-c)]^2}\right]\right.$$
$$+\frac{\beta\tilde{c}_s^2+F_c^2[\bar{u}-(1-\mathrm{Ro}\bar{u}_y)(\bar{u}-c)]}{\tilde{c}_s^2-[M(\bar{u}-c)]^2}$$
$$\left.-\alpha^2(\bar{u}-c)\right]V=0, \tag{3.5}$$

where the Mach number $M\equiv U/\bar{c}_0=\mathrm{Ro}F_c$ has been introduced and the Rossby number is based on the characteristic shear in the basic flow.

The incompressible equation is recovered in the limit $F_c\to 0$ (and Ro finite):

$$\frac{d}{dy}\left[(\bar{u}-c)\frac{dV}{dy}-\bar{u}_y V\right]+[\beta-\alpha^2(\bar{u}-c)]V=0. \tag{3.6}$$

This equation also describes quasigeostrophic barotropic instability on a β plane (see, e.g., Gill 1982, section 13.6). The nonrotating compressible equation (Blumen 1970) is recovered in the limit (F_c, β) $\to 0$ (but with M finite):

$$\frac{d}{dy}\left[\frac{\tilde{c}_s^2\left\{(\bar{u}-c)\frac{dV}{dy}-\bar{u}_y V\right\}}{\tilde{c}_s^2-[M(\bar{u}-c)]^2}\right]-\alpha^2(\bar{u}-c)V=0. \tag{3.7}$$

The compressible quasigeostrophic equation is recovered in the limit Ro $\to 0$:

$$\frac{d}{dy}\left[(\bar{u}-c)\frac{dV}{dy}-\bar{u}_y V\right]$$
$$+\left[\beta-\left(\alpha^2+\frac{F_c^2}{\tilde{c}_s^2}\right)(\bar{u}-c)+\frac{F_c^2}{\tilde{c}_s^2}\bar{u}\right]V=0. \tag{3.8}$$

The last equation is similar to that of the quasigeostrophic shallow water system investigated by Stern (1961) and Lipps (1963) with F_E replaced by F_c, and can be reduced to that in the divergent barotropic model examined by Wiin-Nielsen (1961) with F_I replaced by F_c. The y variation of $\tilde{c}_s^2$ included here is analogous to the y variation of the basic-state depth in the shallow water system.

Lipps's analysis of the shallow water equations showed that growth rates of unstable barotropic modes decrease as F_E increased from 0, that is, as the length scale of the motion approaches the external deformation radius $\sqrt{gH}/f_0$. In this regime, surface displacements and the contribution of vortex tube stretching (associated with horizontal convergence) to the shallow water potential vorticity dynamics are important (Pedlosky 1987). Work is done against gravity to raise the free surface, thereby increasing perturbation potential energy and diminishing the growth rate of barotropic instability (Stern 1961). Conversely, as F_E becomes small, the contribution of surface displacements to the potential vorticity diminishes. When $F_E=0$, a rigid lid is effectively in place, there is no perturbation potential energy or horizontal divergence, and the flow behaves as if it were incompressible.

Compressibility introduces a finite external deformation radius c_0/f_0, which is the distance an acoustic signal travels in one inertial period. In direct analogy to shallow water flow, barotropic growth rates will diminish as F_c increases with compressibility. In this case, the work done against the elastic force during compression is given by $-\varphi'\nabla\cdot(\bar{\rho}\mathbf{v}')$ and represents the sole source of perturbation internal energy and a sink of perturbation kinetic energy when convergence and pressure perturbations are positively correlated. Clearly, this correlation must hold in an unstable normal mode since the internal energy will grow exponentially. Because it is the perturbation momentum flux that drives the conversion from basic state to perturbation kinetic energy, the growth will be slower with this kinetic energy sink. Both compressibility in the present case and free-surface displacements in the shallow water case represent increases of total perturbation available potential energy produced by conversion of basic-state kinetic energy in the barotropic flow (Blumen 1970), and in both cases the ratio of the perturbation available potential energy to the perturbation kinetic energy is provided by the corresponding value of F^2.

Growth rates of the most unstable subsonic barotropic modes in a bounded linear shear layer are shown as a function of Ro and F_c in Fig. 1. The basic flow is shown in Fig. 4.4c of Drazin and Reid (1981), and the shear layer used here is 1/6 as wide as the channel. All growth rates correspond to a wavelength of 7680 km, the most unstable mode in the incompressible problem. The incompressible growth rates ($F_c=0$) are calculated analytically with Eq. (23.8) in Drazin and Reid. The compressible growth rates ($F_c>0$) are derived from the eigenvalues of the linear operator formed by the discretization in space and time of (3.1)–(3.4). The discretization is identical to that used in the full nonlinear model described in the appendix.

For small values of F_c, the growth rates increase approximately linearly with Ro, reflecting the linear dependence of the incompressible growth rates on the magnitude of the basic state shear [Gill 1982, Eq. (13.6.11)]. Growth rates decrease as F_c increases, according to the above discussion. For example, at Ro = 0.1, the growth rate decreases by about 60% as F_c in-

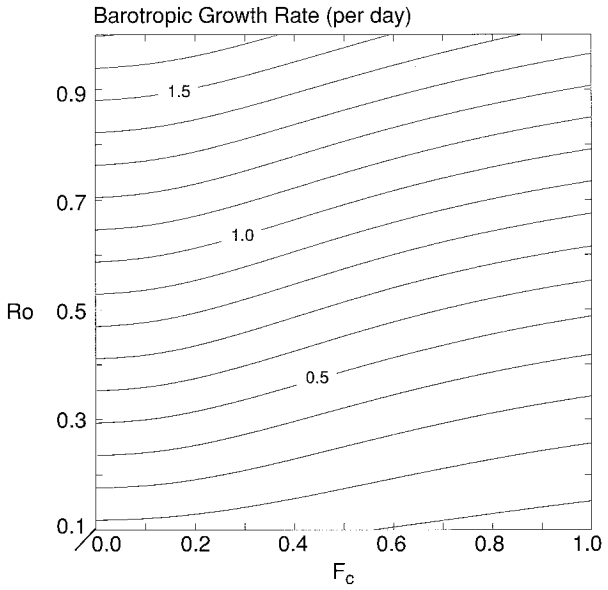

FIG. 1. Growth rates (contoured every 0.1 day^{-1}) for the most unstable barotropic mode corresponding to a bounded shear flow, as a function of (Ro, F_c).

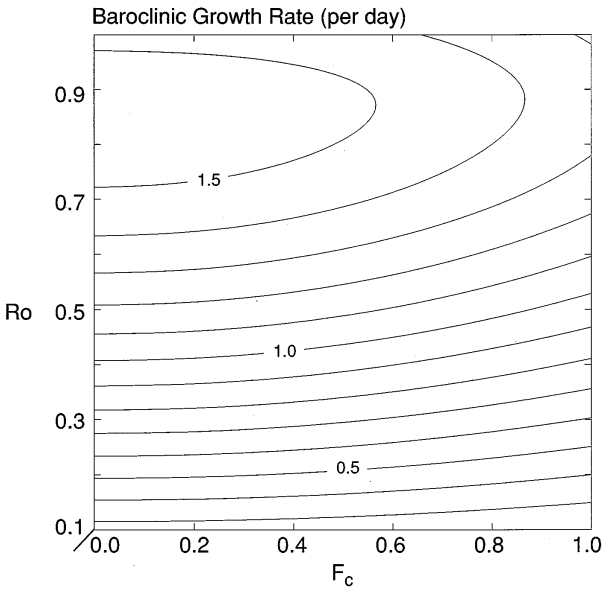

FIG. 2. Growth rates (per day, contoured every 0.05 day^{-1}) for the most unstable baroclinic Eady mode, as a function of (Ro, F_c).

creases from 0 to 1. This decrease is more rapid when the Rossby number is large, and Blumen (1970) has calculated zero growth rates at $M = 1$ for the hyperbolic tangent velocity profile in nonrotating compressible flow.

4. Baroclinic modes

Two-dimensional perturbations to an isothermal geostrophic flow $\bar{\boldsymbol{u}}(z) = \Lambda z$ on an f plane bounded by a rigid lid at height H satisfy

$$\mathrm{Ro}Du' = -\frac{\partial}{\partial x}\varphi' + v' - \mathrm{Ro}w' \tag{4.1}$$

$$\mathrm{Ro}Dv' = -u' \tag{4.2}$$

$$\left(\frac{H}{L}\right)^2 \mathrm{Ro}Dw' = -\frac{\partial}{\partial z}\varphi' + b' \tag{4.3}$$

$$F_c^2\mathrm{Ro}D\varphi' = -\frac{\partial}{\partial x}u' - \frac{\partial}{\partial z}w' + F_c^2\mathrm{Ro}v' + \frac{F_c^2}{F_E^2}w' \tag{4.4}$$

$$\mathrm{Ro}Db' = -w' + \mathrm{Ro}v', \tag{4.5}$$

where $\varphi' = \bar{\theta}P'$. The scaling of Nakamura (1988) has been adopted so that $F_I = 1$ and the Rossby number is now $\mathrm{Ro} = \mathrm{Ri}^{-1/2} \equiv \Lambda/N$, where Ri is the Richardson number. The term proportional to $\varphi' F_E^2$ in (4.3) has been neglected consistent with the assumption that $\mathrm{Ro}F_E^2 \ll 1$. Assuming solutions of the form

$$[u', v', w', \varphi', b'] = [U, V, W, \Phi, B](z)e^{i\alpha(x-ct)} \tag{4.6}$$

results in a single equation for W:

$$(\bar{u} - c)\frac{d}{dz}\left(\frac{L\{W\}}{\Gamma} - \mathrm{Ro}^2\left[\alpha^2(z-c)^2\frac{L\{W\}}{\Gamma} - W\right]\right) - \frac{L\{W\}}{\Gamma} + \left[1 - \left(\frac{H}{L}\right)^2\mathrm{Ro}^2\alpha^2(z-c)^2\right]W = 0, \tag{4.7}$$

where

$$L\{W\} = \frac{dW}{dz} - F_c^2\left[\frac{1}{F_E^2} + \mathrm{Ro}^2(z-c)\right]W \tag{4.8}$$

and

$$\Gamma = -(z-c)\alpha^2 - F_c^2[1 - z - \mathrm{Ro}^2\alpha^2(z-c)^2]. \tag{4.9}$$

In the hydrostatic, Boussinesq limit (H^2/L^2, F_c^2) $\to 0$, (4.7) reduces to Eq. (19) of Nakamura (1988).

Growth rates for a range of Ro and F_c are shown in Fig. 2. The values for $F_c = 0$ in the range $0 \le \mathrm{Ro} \le 0.26$ correspond to those shown in Fig. 1a of Nakamura (1988). The values for $F_c > 0$ are derived from the eigenvalues of the linear operator formed by the discretization of (4.1)–(4.6). For the range of Ro shown in Fig. 2, growth rates of baroclinic modes decrease as a consequence of compressibility for the reasons discussed in the previous section on barotropic modes. However, baroclinic instability in the earth's atmosphere is relatively insensitive to compressibility; typical atmospheric values of the sound speed and deformation radius for baroclinic modes yield $F_c = 0.32$ and the growth rate for $\mathrm{Ro} = 0.1$ decreases only by about 5% from its incompressible value.

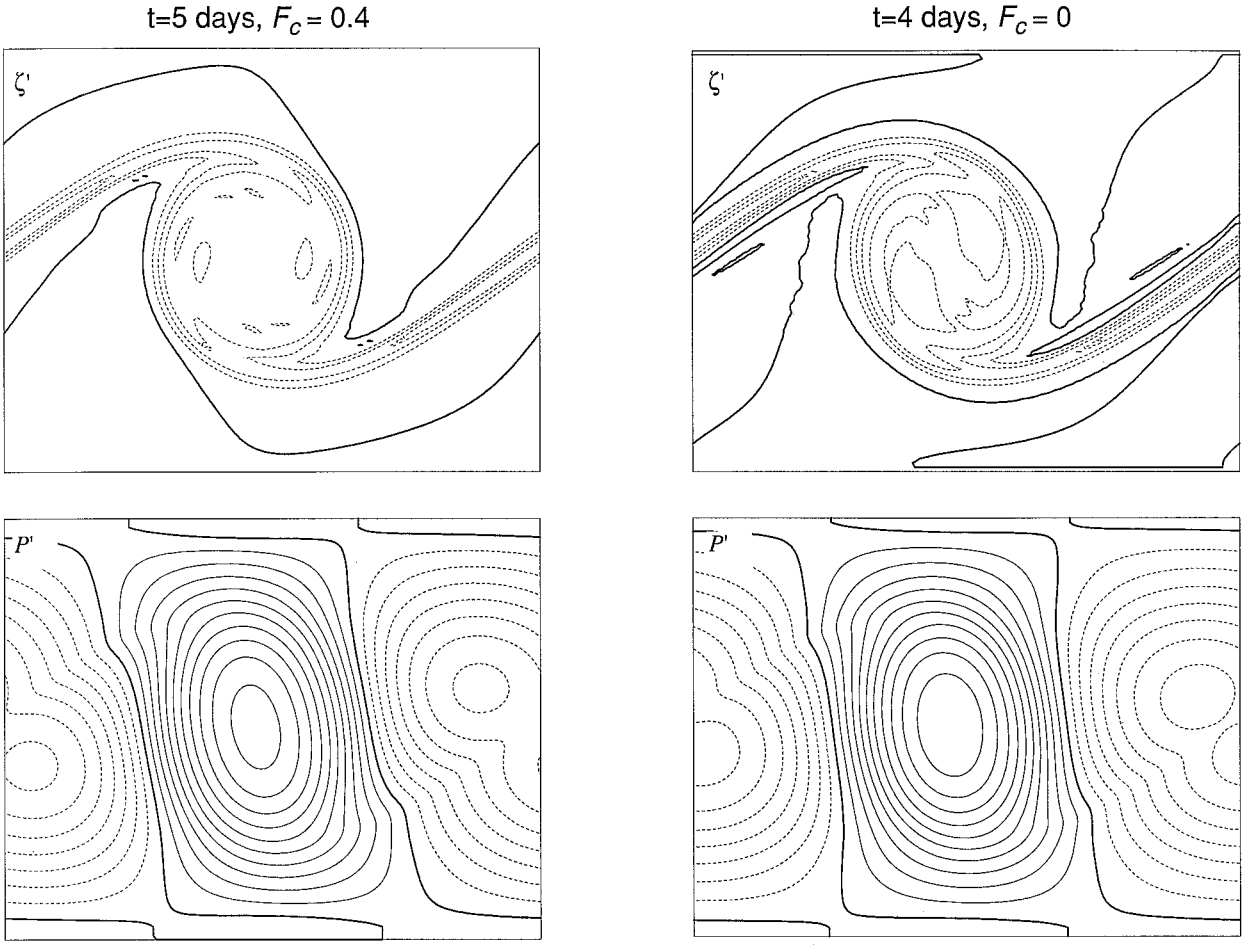

FIG. 3. Vorticity (top, contoured every 1×10^{-5} s^{-1}) and perturbation pressure P' (bottom, contoured every 0.5 J kg^{-1}-K^{-1}) for the compressible barotropic solution after five days of integration (left) and incompressible solution after four days of integration (right). Dashed contours indicate negative values and the bold contour corresponds to zero. The channel has a zonal length of 7680 km wide and is 6000 km wide. The horizontal resolution is 60 km, and the temporal resolution is 60 s in the compressible solution and 180 s in the incompressible one. The zonal average of P' has been subtracted from the bottom panels.

5. Nonlinear simulations

The effects of compressibility on the growth rates of unstable barotropic and baroclinic modes are evident in fully nonlinear simulations of these instabilities when compared to their incompressible counterparts. Such simulations were performed with a new nonhydrostatic compressible version of the ZETA model (Orlanski and Gross 1994) and compared with the solutions provided by the original Boussinesq version of the ZETA model. Unique features of the new model include the use of the terrain-following vertical coordinate Z (Orlanski and Gross 1994) and the retention of all terms in the continuity equation. A complete description of the model is provided in the appendix.

The compressible and incompressible barotropic solutions on an f plane, shown in Fig. 3, are quite similar in the distribution and amplitude of the perturbation pressure and vorticity fields. However, the compressible solution, corresponding to (Ro, F_c) = (0.1, 0.4) is shown after five days of integration, while the incompressible solution is shown after only four days. This clearly shows that the effects of the slower growth rate are felt well into the nonlinear regime. The difference in integration times is consistent with the difference in growth rates of about 25%. All other features of the barotropic roll-up seem well represented in the compressible solution; its development is simply slower than the incompressible one.

Compressible and incompressible simulations of a three-dimensional baroclinic wave on a cosine jet are shown in Fig. 4. The wavelength is 4600 km and the Brunt–Väisälä frequency is $N = 1.15 \times 10^{-2}$ s^{-1}, corresponding closely to the most unstable two-dimensional baroclinic mode discussed by Nakamura (1988). The compressible and incompressible solutions possess quite similar features in the surface vorticity and potential temperature distributions. In particular, frontal strengths and positions compare well between the two

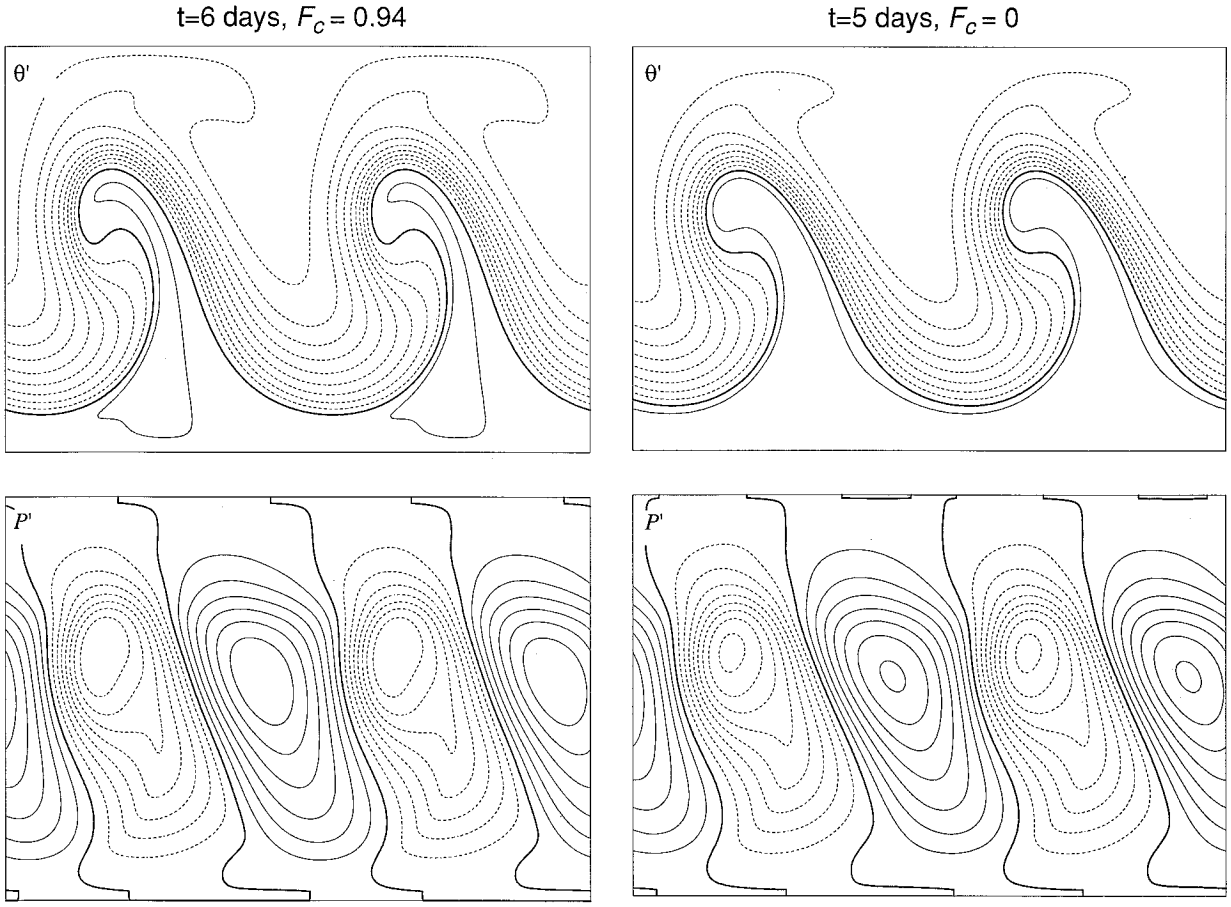

FIG. 4. Surface perturbation potential temperature (top, contoured every 2.0 K) and perturbation pressure P' (bottom, contoured every 1.0 J kg^{-1}-K^{-1}) for the compressible baroclinic wave after six days of integration (left) and incompressible wave after five days of integration (right). Dashed contours indicate negative values and the bold contour corresponds to zero. The channel has a zonal length of 9200 km wide and is 6100 km wide. The horizontal resolution is 48 km, and the temporal resolution is 60 s in the compressible solution and 300 s in the incompressible one. The zonal average of P' has been subtracted from the bottom panels.

solutions. Here, the compressible model has been integrated for six days and corresponds to (Ro, F_c) = (0.27, 0.94), and the incompressible solution has been integrated for five days; two-dimensional growth rates for these parameter values differ by about 20% according to Fig. 2. As in the barotropic integration, the development of the compressible baroclinic solution is simply slower than the incompressible one.

6. Conclusions

Linear growth rates have been calculated for barotropic and two-dimensional baroclinic instability in a compressible atmosphere. Compressibility introduces a deformation radius based on the acoustic phase speed, and the effects of compressibility depend on the ratio of length scales $F_c = f_0 L/c_0$. Growth rates decrease with compressibility because the work done by compression represents a source of perturbation internal energy and a sink of perturbation kinetic energy, which have a ratio of F_c^2 in the unstable linear modes. The diminished growth rates are also evident in fully nonlinear simulations of these instabilities with a new nonhydrostatic compressible mesoscale model.

One consequence of this sensitivity to compressibility is that numerical models that increase efficiency by explicitly decreasing the sound speed may provide artificially slow baroclinic and barotropic growth by indirectly increasing the compressibility of the medium. According to the analysis presented above, however, this detrimental effect will diminish as the scale of the relevant feature decreases relative to the deformation radius.

Acknowledgments. The author gratefully acknowledges Isidoro Orlanski, who pointed out the similarity between the linearized barotropic compressible and shallow water equations and provided the reference to Lipps's early work on divergent barotropic flow. Dr. Orlanski and Dr. Stephen Garner also provided many useful discussions and comments on this work. The

comments of two anonymous reviewers were very helpful in clarifying the original version of this paper.

APPENDIX

The Nonhydrostatic Compressible ZETA Model

The nonhydrostatic compressible primitive equation model used in the simulations presented in section 5 is an extension of the hydrostatic ZETA model described in the appendix of Orlanski and Gross (1994). The terrain-following ZETA coordinate is given by

$$Z = \exp\left[-\epsilon\left(\frac{z - h(x, y)}{H - h(x, y)}\right)\right], \tag{A.1}$$

where z is physical height, $h(x, y)$ represents the height profile of the topography, and H is the height of the model rigid lid. Larger values of ϵ place more model levels and higher resolution near the ground.

a. Governing equations

The governing equations (2.1)–(2.4) expressed in the ZETA coordinate (A.1) are the momentum equations,

$$\frac{\partial \mathbf{v}_H}{\partial t} = \mathbf{F}_H, \tag{A.2}$$

$$\frac{\partial \omega}{\partial t} = -\bar{\theta}\left[\frac{1}{\delta_Z}\frac{\partial}{\partial Z}P'\right] + F_\omega, \tag{A.3}$$

expressed in terms of the horizontal velocity $\mathbf{v}_H$ and the vertical velocity

$$\omega = \delta_Z \dot{Z} = w - \mathbf{v}_H \cdot \nabla z, \tag{A.4}$$

the continuity equation expressed in terms of the Exner function $P \equiv c_p(p/p_0)^{R/c_p}$,

$$\frac{\partial}{\partial t}P' = \frac{\bar{c}_s^2}{\bar{\rho}\bar{\theta}^2}\frac{1}{\delta_Z}\frac{\partial}{\partial Z}\bar{\rho}\bar{\theta}\omega + F_P, \tag{A.5}$$

and the thermodynamic equation expressed in terms of potential temperature θ,

$$\frac{\partial \theta}{\partial t} = F_\theta. \tag{A.6}$$

The explicit forcing terms are given by

$$\mathbf{F}_H = -\theta\left(\nabla P' - \left[\frac{1}{\delta_Z}\frac{\partial}{\partial Z}P'\right]\nabla z\right) - f\,\mathbf{k} \times \mathbf{v}_H - \mathbf{A}_{\mathbf{v}_H} + \mathbf{D}_{\mathbf{v}_H}, \tag{A.7}$$

$$F_\omega = \frac{g\theta'}{\bar{\theta}} - \theta'\left[\frac{1}{\delta_Z}\frac{\partial}{\partial Z}P'\right] - A_w - \frac{\partial \mathbf{v}_H}{\partial t}\cdot\nabla z + D_w, \tag{A.8}$$

$$F_P = -\frac{\bar{c}_s^2}{\bar{\rho}\bar{\theta}^2}\frac{1}{\delta_Z}\nabla\cdot(\bar{\rho}\bar{\theta}\mathbf{v}_H\delta_Z) - \frac{R}{c_v}P'\left(\frac{1}{\delta_Z}\nabla\cdot\mathbf{v}\delta_Z\right) - A_{P'} + \left(\frac{\bar{c}_s^2}{\bar{\theta}} + \frac{R}{c_v}P'\right)\frac{Q}{\theta}, \tag{A.9}$$

$$F_\theta = -A_\theta + Q. \tag{A.10}$$

An overbar denotes a static hydrostatic state satisfying $\partial\bar{P}/\partial Z = -g\delta_z/\bar{\theta}$ and a prime denotes deviations from this state. In particular, the static-state pressure has been removed from the pressure gradient in (A.2) and (A.3) to minimize cancellation between the two pressure gradient terms in (A.7) and the hydrostatic balance of the static state in (A.3). The geometric conversion factor is given by

$$\frac{\partial z}{\partial Z} \equiv \delta_Z = -\frac{(H - h(x, y))}{\epsilon Z}, \tag{A.11}$$

and A indicates advection in the Z coordinate system:

$$A_f = \mathbf{v}_H\cdot\nabla f + \omega\frac{1}{\delta_Z}\frac{\partial f}{\partial Z} = \mathbf{v}_H\cdot\nabla f + \dot{Z}\frac{\partial f}{\partial Z}. \tag{A.12}$$

In the dry model used here, momentum dissipation D and heating Q are parameterized by fourth-order horizontal diffusion and a vertical mixing scheme based on the local Richardson number (Ross and Orlanski 1982). For efficiency, the advection and dissipation terms in (A.8) operate on w rather than ω. The boundary conditions are similar to those imposed in the hydrostatic model: vertical walls at the north and south boundaries, a flat rigid lid, and periodicity in the zonal direction.

b. Discrete equations

The nonhydrostatic compressible model uses the same Arakawa C-grid and leapfrog time-differencing schemes as the hydrostatic model; however, the explicit representation of sound waves practically requires the use of an implicit scheme for integrating vertically propagating acoustic waves. The discrete equations are given by

$$u_H^{n+1} = u_H^{n-1} + 2\Delta t F_u^n, \tag{A.13}$$

$$v_H^{n+1} = v_H^{n-1} + 2\Delta t F_v^n, \tag{A.14}$$

$$\langle \omega_{k+1/2} \rangle = \omega_{k+1/2}^{n-1} + \Delta t F_\omega^n - \Delta t \overline{\left(\frac{\bar{\theta}}{\delta_Z}\right)}^Z \Delta_Z \langle P'_{k+1} \rangle, \tag{A.15}$$

$$\langle P'_k \rangle = P'^{n-1}_k + \Delta t F_P^n - \frac{\Delta t}{\Delta Z}[\gamma_k^+ \langle \omega_{k+1/2} \rangle - \gamma_k^- \langle \omega_{k-1/2} \rangle], \tag{A.16}$$

$$\theta_H^{n+1} = \theta_H^{n-1} + 2\Delta t F_\theta^n, \tag{A.17}$$

where the discretized forcing terms are

$$F_u^n = -\overline{\theta^n}^x \left(\Delta_x P'^n - \overline{\left[\frac{\Delta_Z P'^n}{\overline{\delta_Z}^Z}\right]}^{xz} \Delta_x z \right) - f\overline{v^n}^{xy} - \left(\overline{\overline{u^n}^x \Delta_x u^n}^x + \overline{\overline{v^n}^x \Delta_y u^n}^y + \overline{\overline{\omega^n}^x \Delta_Z u^n}^z \right) + D_u^{n-1}, \tag{A.18}$$

$$F_v^n = -\overline{\theta^n}^y \left(\Delta_y P'^n - \overline{\left[\frac{\Delta_Z P'^n}{\overline{\delta_Z}^Z}\right]}^{yz} \Delta_y z \right) - f\overline{u^n}^{xy} - \left(\overline{\overline{u^n}^y \Delta_x v^n}^x + \overline{\overline{v^n}^y \Delta_y v^n}^y + \overline{\overline{\omega^n}^y \Delta_Z v^n}^z \right) + D_v^{n-1}, \tag{A.19}$$

$$F_\omega^n = \frac{\overline{g\theta'^n}^Z}{\bar{\theta}} - \overline{\theta'^n}^z \frac{\Delta Z P'^n}{\overline{\sigma_Z}^z} - F_u^n \Delta_x z - F_v^n \Delta_y z - \left(\overline{\overline{u^n}^Z \Delta_x w^n}^x + \overline{\overline{v^n}^Z \Delta_y w^n}^y + \overline{\overline{\omega^n}^z \Delta_Z w^n}^z \right) + D_w^{n-1}, \tag{A.20}$$

$$F_P = -\frac{\bar{c}_s^2}{\bar{\rho}\bar{\theta}^2} \frac{1}{\delta_Z} \left(\Delta_x \overline{\bar{\rho}\theta \delta_Z}^x u^n + \Delta_y \overline{\bar{\rho}\theta \delta_Z}^y v^n \right) - \frac{R}{c_v} \frac{P'^n}{\delta_Z} \left(\Delta_x \overline{\delta_Z}^x u^n + \Delta_y \overline{\delta_Z}^y v^n + \Delta_Z \omega^n \right) - \left(\overline{u^n \Delta_x P'^n}^x + \overline{v^n \Delta_y P'^n}^y + \overline{\omega^n \Delta_Z P'^n}^z \right) + \left(\frac{\bar{c}_s^2}{\bar{\theta}} + \frac{R}{c_v} P'^n \right) \frac{Q}{\theta^n}, \tag{A.21}$$

$$F_\theta^n = -\left(\overline{u^n \Delta_x \theta^n}^x + \overline{v^n \Delta_y \theta^n}^y + \overline{\omega^n \Delta_Z \theta^n}^z \right) + Q, \tag{A.22}$$

the coefficient in (A.16) is

$$(\gamma_k^+, \gamma_k^-) = \left(\frac{\bar{c}_s^2}{\bar{\rho}\bar{\theta}^2} \frac{1}{\delta_Z} \right)_k \left(\overline{[\bar{\rho}\bar{\theta}]_k}^Z, \overline{[\bar{\rho}\bar{\theta}]_{k-1}}^Z \right), \tag{A.23}$$

and the finite-difference operators

$$\langle q \rangle = \frac{1}{2}(q^{n+1} + q^{n-1}), \tag{A.24}$$

$$\bar{q}^x = \frac{1}{2}(q_{i+1jk} + q_{ijk}), \tag{A.25}$$

$$\Delta_x q = \frac{1}{\Delta x}(q_{ijk} - q_{i-1jk}). \tag{A.26}$$

may be applied to any variable q. Similar averaging and differencing operators may be derived for the other independent variables. Since the boundary conditions for ω are so well posed [$\omega = 0$ at $Z = (1, e^{-\epsilon})$], the pressure is eliminated from (A.15) to (A.16), resulting in a single tridiagonal equation for $\langle \omega \rangle$. The remaining variables may be found by means of (A.13–A.14) and (A.16–A.17).

REFERENCES

Blumen, W., 1970: Shear layer instability of an inviscid compressible fluid. *J. Fluid Mech.,* **40,** 769–781.

Chen, C., 1991: A nested grid, nonhydrostatic, elastic model using a terrain-following coordinate transformation: The radiative-nesting boundary conditions. *Mon. Wea. Rev.,* **119,** 2852–2869.

Drazin, P. G., and W. H. Reid, 1982: *Hydrodynamic Stability.* Cambridge University Press, 527 pp.

Gill, A. E., 1982: *Atmosphere–Ocean Dynamics.* Academic Press, 662 pp.

Held, I. M., R. S. Hemler, and V. Ramaswamy, 1993: Radiative-convective equilibrium with explicit two-dimensional moist convection. *J. Atmos. Sci.,* **50,** 3909–3927.

Lipps, F. B., 1963: Stability of jets in a divergent barotropic fluid. *J. Atmos. Sci.,* **20,** 120–129.

Nakamura, N., 1988: Scale selection of baroclinic instability—Effects of stratification and nongeostrophy. *J. Atmos. Sci.,* **45,** 3253–3267.

Orlanski, I., and B. D. Gross, 1994: Orographic modification of cyclone development. *J. Atmos. Sci.,* **51,** 589–611.

Pedlosky, J., 1987: *Geophysical Fluid Dynamics.* 2d ed. Springer-Verlag, 710 pp.

Ross, B. B., and I. Orlanski, 1982: The evolution of an observed cold front. Part I: Numerical simulation. *J. Atmos. Sci.,* **39,** 296–327.

Stern, M. E., 1961: The stability of themoclinic jets. *Tellus,* **13,** 503–508.

Wiin-Nielsen, A., 1961: On short- and long-term variations in quasi-barotropic flow. *Mon. Wea. Rev.,* **89,** 461–476.